Width of Atomic L_2 and L_3 Vacancy States near $Z=30$

Lo I Yin and Isidore Adler
NASA-Goddard Space Flight Center, Code 641, Greenbelt, Maryland 20771

Mau Hsiung Chen* and Bernd Crasemann*
Department of Physics, University of Oregon, Eugene, Oregon 97403
(Received 8 November 1972)

Consequences of the discontinuity at $Z=30$ in the Coster–Kronig transition probability f_{23} have been investigated by Auger and photoelectron spectroscopy. The L_3-$M_{45}M_{45}/L_2$-$M_{45}M_{45}$ Auger intensity ratio is found to undergo a sudden decrease at $Z=30$. Relative L_2 and L_3 level widths of Cu and Zn are derived from photoelectron spectra; while the L_3 width increases from Cu to Zn, the L_2 width of Cu is greater than that of Zn, contrary to the general trend. The data agree qualitatively with earlier calculations of radiationless-transition probabilities based on hydrogenic wave functions, but substantial quantitative discrepancies are found. New calculations have been performed with numerical single-particle wave functions based on Green's atomic independent-particle model. With suitable assumptions regarding Cu and Zn M_4 and M_5 electron binding energies in the presence of an L_2 vacancy, reasonable agreement between calculated and observed Auger-electron intensity ratios and L-subshell level widths is attained.

I. INTRODUCTION

Comprehensive calculations of radiative,[1–4] Auger,[4–8] and Coster–Kronig[4–7] transition probabilities to atomic L-shell vacancies have recently been completed, leading to a set of theoretical partial and total level widths and fluorescence yields for a wide range of atomic numbers.[9,10] On the other hand, experimental information on these quantities[11–23] has essentially been restricted to atomic numbers above $Z\cong 65$, owing to limitations of the resolution of solid-state detectors employed in x-ray coincidence measurements from which the most reliable information had been derived. However, it now is possible to utilize high-resolution Auger and photoelectron spectroscopy to measure aspects of atomic inner-shell vacancy decay that can be used to check theoretical results at low Z.[24,25] In this paper, we report on an investigation of the discontinuity in the L_2 level width and the L_3-$M_{45}M_{45}/L_2$-$M_{45}M_{45}$ Auger intensity ratio at $Z=30$, which can be traced to a discontinuity in the Coster–Kronig transition probability f_{23} predicted in earlier calculations.[5] The results of a more refined computation are described and compared with the experimental data.

II. EXPERIMENTS

A. Instrumentation

The details of our x-ray photoelectron spectrometer were reported elsewhere.[26] The entire assembly is situated in an oil-free vacuum system with an operating pressure of about 1×10^{-8} Torr. Spec-pure foils of Co, Ni, Cu, and Zn were used as samples and both Al $K\alpha_{1,2}$ and Mg $K\alpha_{1,2}$ x rays were used for excitation. Because the electrons of interest originate from the top tens of angstroms of the sample surface, the samples were sputter-cleaned with Ar ions at 1.5 kV, 20 μm pressure, and a current density of about 0.2 mA/cm^2, in an antechamber prior to measurements. The time interval between the end of ion sputtering and the beginning of analysis at 5×10^{-8} torr was ~6 min. An 11-cm-radius hemispherical electrostatic spectrometer was used to analyze the electron energies. High resolution was achieved by reducing the energies of the electrons from the sample to about 60 eV before they enter the spectrometer.[27] The electrons were then pulse counted and their energy distribution recorded on a multichannel analyzer operated in the multiscaler mode. Energy calibration of the Auger spectra was achieved by using the photoelectron lines from the sample.[27] In this manner, the work function of the spectrometer was implicitly taken into account.

In the present experiment, although the relative level widths are more important than the absolute widths, an effort was made to measure the absolute widths as well. For these measurements the absolute resolution of the spectrometer was improved progressively by reducing the energy of the electrons entering the spectrometer[27] at the expense of reduced intensities. Such a procedure was continued until the FWHM (full width at half-maximum) of the Al $K\alpha_{1,2}$-excited N_7 ($4f_{7/2}$) photoelectron line of Au was reduced to a minimum value of 1.31 eV. Additional improvement of the spectrometer resolution had no further effect. Since to our knowledge this minimum value is also the lowest value achieved in other ESCA instru-

ments using nonmonochromatized Al $K\alpha_{1,2}$ radiation, it is most likely that at such spectrometer settings the instrumental contribution to the total photoelectron linewidth can be considered negligible. Furthermore, all the experimental photoelectron linewidths of interest (corresponding to the L_2 and L_3 levels of Cu and Zn) are greater than 1.3 eV. To ensure reproducibility, each level width was measured at three different occasions, using three different samples of the same element.

For the measurements of relative intensities, the spectrometer resolution was degraded somewhat, in order to reduce data-collection time, such that the FWHM of the Al $K\alpha_{1,2}$-excited Au N_7 line was 1.46 eV.

B. Treatment of Data

The width of an experimental x-ray photoelectron line includes contributions from the incident x-ray width, the width of the level from which photoelectrons are ejected, and the instrumental width. As mentioned in Sec. II A, our instrumental contribution is reduced to a minimum and kept constant. However, small energy losses of the emerging electrons tend to produce a background which distorts the low-energy side of the line and causes broadening of the observed width. This background must be subtracted from the experimental data. To this end, a spline-fit computer program was used to smooth the data; then a fourth-degree polynomial was generated to fit the background on both sides of the photoelectron peak so that it extends smoothly through the peak region itself. The FWHM of the background-subtracted peak was then measured and the results were plotted by a CalComp-780 plotter. An example of this procedure is illustrated in Fig. 1, in which the CalComp plots of the N_6, N_7 doublet of Au and the L_3 peak of Cu using Al $K\alpha_{1,2}$ x rays are shown. After background subtraction, the shape of the L_3 peak of Cu is seen to be quite symmetrical. In fact, a detailed fit shows that its shape is intermediate between a Lorentzian and a Gaussian. The FWHM of the Au N_7 peak measured in this manner is 1.31 eV, and that of the Cu L_3 peak is 1.44 eV.

The approximate relative intensities of the Auger and photoelectron lines were derived in a much less rigorous manner by using a planimeter.

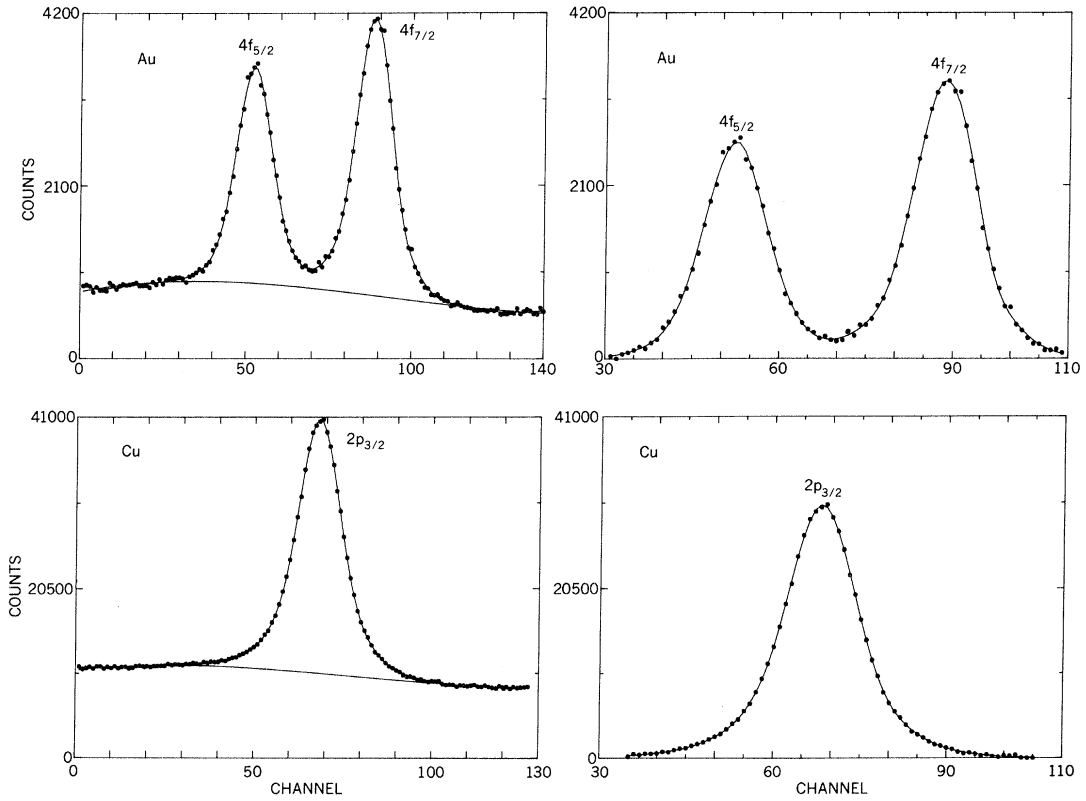

FIG. 1. CalComp plots of measured electron spectra, illustrating smoothing by a spline-fit computer program and background generated by fourth-degree polynomials. Top: Al $K\alpha_{1,2}$-excited photoelectron spectrum of the N_6 and N_7 ($4f_{5/2}$, $4f_{7/2}$) doublet of Au. Bottom: Al $K\alpha_{1,2}$-excited photoelectron line of the L_3 ($2p_{3/2}$) level of Cu. Left: prior to background subtraction. Right: after background subtraction. FWHM of the Au N_7 line is 1.31 eV, and FWHM of the Cu L_3 line, 1.44 eV. Units on the abscissa are 0.1 eV/channel.

TABLE I. Experimental L_2- and L_3-subshell level widths $\Gamma(L_i)$ for $_{29}$Cu and $_{30}$Zn. All widths are given in eV.

Element	$\Gamma(L_2)$	$\Gamma(L_3)$
$_{29}$Cu	0.98 ± 0.04	0.54 ± 0.03
$_{30}$Zn	0.84 ± 0.04	0.66 ± 0.03

C. Results

1. Level Width

Taking the combined x-ray width of the Al $K\alpha_{1,2}$ lines to be 0.9 eV[28] and that of the Mg $K\alpha_{1,2}$ lines to be 0.8 eV,[29] and assuming that the width of a photoelectron line is the Lorentzian sum of the x-ray width and the level width of interest, with negligible instrumental broadening, the results of the deduced L_2- and L_3-level widths of $_{29}$Cu and $_{30}$Zn are as listed in Table I. The quoted errors reflect only experimental uncertainties. They do not include systematic errors such as the accuracy of the assumed x-ray widths or the small instrumental contribution to the measured widths. We note that our value of 0.54 eV for the L_3-level width of Cu compares quite favorably with that of 0.5 eV, quoted by Parratt.[30] Of importance here is the result that, whereas the L_3-level width of $_{30}$Zn is greater than that of $_{29}$Cu, the relative width of the L_2 levels shows exactly the opposite trend.

2. Relative Intensities

Figure 2 shows the Al $K\alpha_{1,2}$-excited photoelectron spectra of the L_2 and L_3 levels of Co through Zn ($27 \leq Z \leq 30$). The various features of the spectra are interpreted in Refs. 31–33. For the present purpose, it suffices to note that in all four samples the L_3/L_2 intensity ratio is essentially 2, proportional to the electron population ratio of these levels.

The L_3-$M_{45}M_{45}$ and L_2-$M_{45}M_{45}$ portions of the LMM Auger spectra of the same elements are shown in Fig. 3. For these elements, this is the most prominent portion of the entire LMM Auger spectrum.[27,33–38] Because this portion lies at the high-energy end of the spectrum, it is relatively free of background, with easily distinguishable

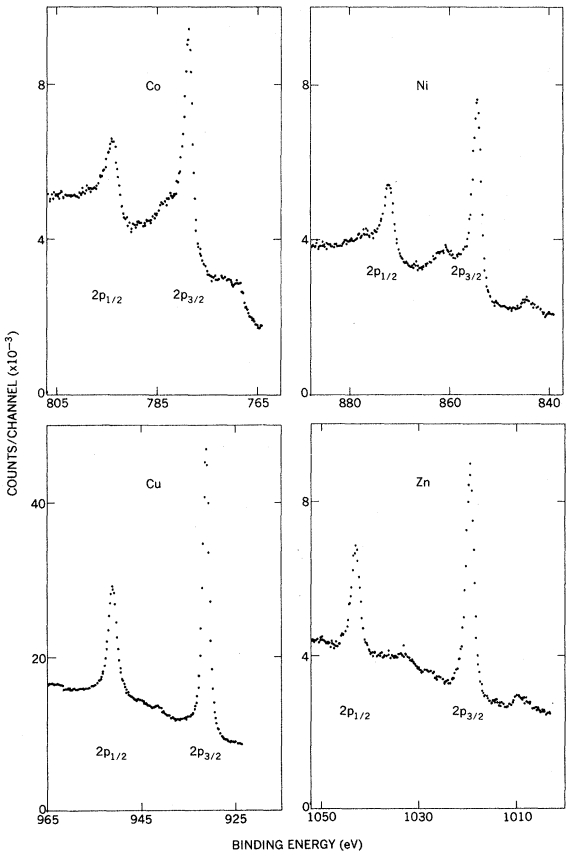

FIG. 2. Al $K\alpha_{1,2}$-excited photoelectron spectra of the L_2 and L_3 ($2p_{1/2}$,$2p_{3/2}$) levels of Co, Ni, Cu, and Zn ($27 \leq Z \leq 30$). The intensity ratio L_3/L_2 is about 2 for all four samples.

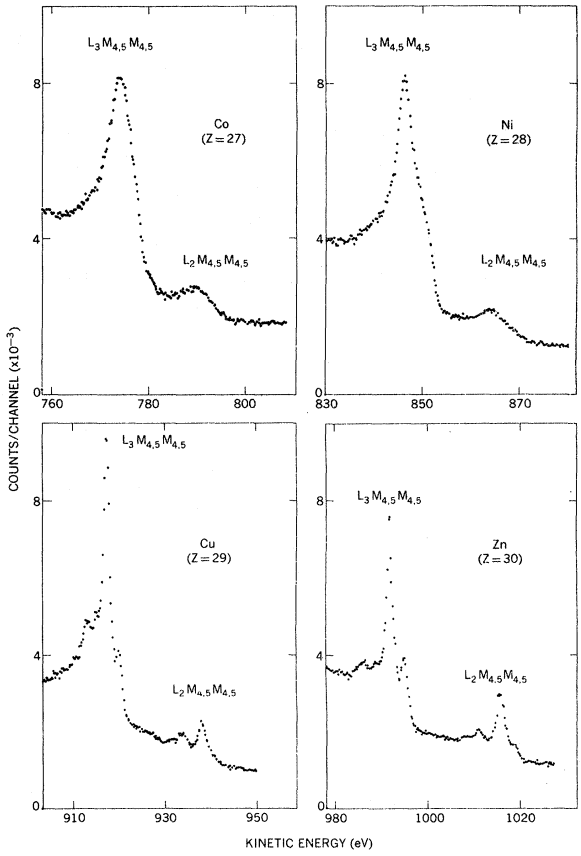

FIG. 3. L_3-$M_{45}M_{45}$ and L_2-$M_{45}M_{45}$ Auger spectra of Co, Ni, Cu, and Zn ($27 \leq Z \leq 30$). The intensity ratio L_3-$M_{45}M_{45}/L_2$-$M_{45}M_{45}$ is not constant and decreases sharply at $Z = 30$.

features. For these reasons, only this part of the spectrum is included here for the determination of relative intensities in connection with the L_2-L_3X Coster–Kronig transitions. Although the fine structures in the Cu and Zn spectra of Fig. 3 have been reported and interpreted previously by some of the present authors in terms of LS coupling of the final outer-shell vacancies,[33] this is the first time that they have been so clearly resolved as a consequence of the improved instrumental resolution.

Figure 3 indicates that, in contrast to the photoelectron spectra, the L_3-$M_{45}M_{45}/L_2$-$M_{45}M_{45}$ intensity ratio is not constant among the four samples. Planimeter integration indicates approximate ratios of ~9 for Ni and Co, ~7 for Cu, and only ~2.5 for Zn. The sudden decrease of this ratio at $_{30}$Zn is of special significance in the present context.

D. Discussion

In Sec. II C, measured intensity ratios in both the Auger and photoelectron spectra for $27 \leq Z \leq 30$ were presented. In general, intensities in the electron spectra of solids depend on a rather complex series of parameters. For instance, the intensity of a photoelectron line depends not only on the photoelectric cross section of the shell from which the electrons originate, but also on the angular distribution of the ejected photoelectrons, the escape probability of such electrons from the sample, a variety of energy-loss mechanisms, and the detection efficiency of the spectrometer-detector system for electrons with this energy. Fortunately, in the present case, we compare L_3 and L_2 photoelectrons which have similar kinetic energies, and the instrumental efficiency is kept constant, so that most of the factors mentioned above are approximately equal. Furthermore, large differences in intensity ratios between the photoelectron spectra and the Auger spectra are compared, so that fine-scale differences have little influence upon the over-all results. Thus, in this instance, the relative L_3- and L_2-photoelectron intensities do give an indication of the relative photoelectric cross sections at the incident x-ray energies, and hence, of the relative initial vacancy distribution in the L_3 and L_2 shells immediately after photoionization. The spectra in Fig. 2 indicate that the initial L_3/L_2-shell vacancy ratio is approximately 2 for all four samples.

The kinetic energies of the L_3-$M_{45}M_{45}$ and L_2-$M_{45}M_{45}$ Auger lines are also similar, their separation being the same as that of the L_3- and L_2-photoelectron lines. Consequently, the various factors mentioned above again cancel when intensity ratios are computed. However, the intensities of the L_i-MM Auger lines also depend on the vacancy distribution in the L_ith subshell at the time of Auger emission and the fluorescence and Auger yields of the L_i subshell. Now it is apparent from the calculations discussed in Sec. III (as well as from other calculations[1,4,9]) that the fluorescence yields ω_3 and ω_2 are both negligible (≤ 0.01) in this Z region, and that the Auger widths $\Gamma_A(L_3)$ and $\Gamma_A(L_2)$ are approximately equal for a given element. Therefore, the L_3-MM/L_2-MM intensity ratio essentially reflects the L_3/L_2 vacancy ratio at the time of Auger emission. This being the case, the observed large L_3-$M_{45}M_{45}/L_2$-$M_{45}M_{45}$ ratios (>>2) in the spectra shown in Fig. 3 indicate that considerable reorganization of vacancies takes place *subsequent* to the photoionization of the L_3 and L_2 shells and *prior* to the emission of Auger electrons. A likely mechanism for such vacancy shifts is that of Coster–Kronig transitions.

Where Coster–Kronig transitions are energetically possible their probabilities are much greater than those of ordinary Auger transitions.[9,39] A primary vacancy can thus be shifted from a lower to a higher subshell before it is filled by an electron from another major shell. Photoelectron spectra that we have measured (not shown here) indicate that the uncorrected L_1-photoelectron intensity is approximately six times lower than the L_3 and L_2 intensities, implying that there are substantially fewer initial vacancies in the L_1 subshell. Previous calculations[4,5,9] have shown that in the vicinity of $Z = 30$ the Coster–Kronig transition probabilities f_{12} and f_{13} vary smoothly with atomic number, and that the ratio f_{13}/f_{12} is close to 2 for each element. Consequently, a number of the initial L_1 vacancies will shift to the L_2 and L_3 shells, twice as many going to the L_3 shell as to the L_2 shell. These shifts will thus somewhat enhance the L_3/L_2 vacancy ratio, and hence, the subsequent L_3-MM/L_2-MM intensity ratio, but the amount of this enhancement will be nearly the same for all four elements which concern us here. Therefore, L_1-L_2X and L_1-L_3X Coster–Kronig transitions alone can account neither for the large observed intensity ratios nor for the sudden decrease of these ratios at $Z = 30$, as illustrated in Fig. 3. These observed features must be associated specifically with the theoretically predicted behavior of the f_{23} Coster–Kronig transition probability.

The results of the level-width measurements listed in Table I provide additional support for the sudden change in f_{23} at $Z = 30$. In the absence of Coster–Kronig transitions, level widths normally increase with increasing Z.[9,31] Such indeed is the case with the measured $\Gamma(L_3)$ of $_{29}$Cu and $_{30}$Zn. However, $\Gamma(L_2)$ shows exactly the opposite trend. This anomalous decrease in $\Gamma(L_2)$ confirms the presence of the predicted discontinuity of f_{23} at $Z = 30$.

Because Co and Ni have unfilled $3d$ shells, broadening effects due to multiplet splitting occur[40];

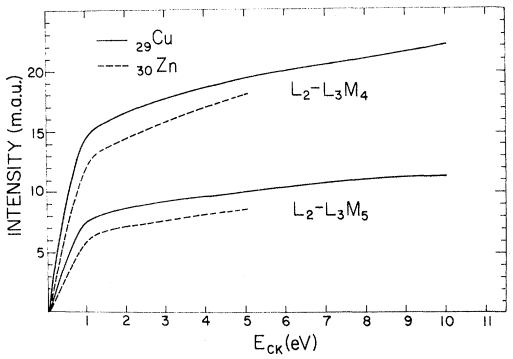

FIG. 4. Theoretical L_2-L_3M_4 and L_2-L_3M_5 Coster–Kronig transition probabilities (in 10^{-3} a.u.) for Cu and Zn, as functions of ejected-electron energy. The calculation is based on Green's analytic potential for the atomic independent-particle model.

these and the presence of excessive energy-loss background (Fig. 2) prevented meaningful measurements of level widths of these two elements.

III. THEORY

A. Calculation of Transition Probabilities

Earlier calculations,[5,6] by some of the present authors, of transition probabilities to L-shell vacancies had been based on analytic hydrogenic wave functions, in order to limit computer-time demands. (It should be noted that as many as 3000 direct and exchange matrix elements must be included in the computation of the total Auger width of an L_3-vacancy state.) The early results are only in qualitative agreement with the data from the experiments described in Sec. II. We now have recalculated L_2- and L_3-shell quantities in the neighborhood of $Z = 30$ with more realistic wave functions.

Radiationless transition probabilities were computed following Wentzel's ansatz.[41] The initial state represented by the two-hole configuration that consists of one inner-shell vacancy and one hole in the continuum undergoes a transition, due to the Coulomb interaction, to the final two-hole configuration that consists of two inner-shell vacancies. Spherical symmetry of the potential is assumed, permitting separation of radial and angular parts of the single-particle wave functions and of the Auger matrix elements.

The single-particle bound-state and continuum radial wave functions required in the Auger calculations were found by solving the radial wave equation numerically with the analytic potential for a neutral atom given by the atomic independent-particle model of Green *et al.*[42] The angular factors of the Auger matrix elements were computed in j-j coupling, which is the most appropriate scheme for the calculation of Coster–Kronig transition probabilities.[43] The radial factors of the Auger matrix elements were obtained by numerical integration. Details of the calculation have been described elsewhere.[44,45] The radiationless transition probabilities computed in the present work were combined with x-ray emission rates calculated by Scofield[1,2] to derive total level widths, fluorescence yields, and Coster–Kronig transition probabilities.

Auger widths $\Gamma_A(L_2)$ and $\Gamma_A(L_3)$ computed here from Green's potential are only one-third as large as those derived from hydrogenic wave functions, but agree closely with the results of test calculations based on the Herman–Skillman[46] Hartree–Slater potential. These widths are ~25% smaller than the results of McGuire,[4] based on solutions of the Schrödinger equation for a piecewise straight-line approximation to the Hermann–Skillman Hartree–Slater potential. Fluorescence yields ω_2 found in the Green-potential calculation exceed those computed from hydrogenic wave functions[5] by 32% for $Z = 26$, 14% for $Z = 28$, and 6% for

TABLE II. Theoretical L_2- and L_3-subshell Auger widths $\Gamma_A(L_i)$, total widths $\Gamma(L_i)$, fluorescence yields ω_i, and L_2-L_3X Coster–Kronig widths $\Gamma(L_2L_3)$ and Coster–Kronig transition probabilities f_{23}. All widths are given in eV. For $Z = 29$ and $Z = 30$, results for the L_2 subshell are listed for three different assumptions regarding the energetics: (a) L_2-L_3-M_4 and L_2-L_3M_5 transitions are possible; (b) L_2-L_3M_5 transitions are possible but L_2-L_3M_4 transitions are not; (c) neither L_2-L_3M_4 nor L_2-L_3M_5 transitions are energetically possible. All calculations are based on Green's atomic independent-particle potential.

	$_{26}$Fe	$_{28}$Ni	$_{29}$Cu			$_{30}$Zn		
	(a)	(a)	(a)	(b)	(c)	(a)	(b)	(c)
$\Gamma_A(L_2)$	0.354	0.465	0.515	0.515	0.515	0.607	0.607	0.607
$\Gamma_A(L_2L_3)$	0.583	0.801	0.922	0.318	0.00476	0.747	0.251	0.0098
$\Gamma(L_2)$	0.939	1.270	1.442	0.838	0.520	1.361	0.865	0.624
ω_2	0.00212	0.00312	0.00381	0.00656	0.0106	0.00525	0.00827	0.0115
f_{23}	0.621	0.631	0.639	0.379	0.00915	0.549	0.230	0.0157
$\Gamma_A(L_3)$			0.546			0.644		
$\Gamma(L_3)$			0.551			0.651		
ω_3			0.00978			0.0108		

TABLE III. Theoretical L_3-$M_{45}M_{45}/L_2$-$M_{45}M_{45}$ Auger-electron intensity ratios for $Z=29$ and $Z=30$, computed on three different assumptions regarding the energetics: (a) L_2-L_3M_4 and L_2-L_3M_5 Coster–Kronig transitions are possible; (b) L_2-L_3M_5 transitions are possible but L_2-L_3M_4 transitions are not; (c) both L_2-L_3M_4 and L_2-L_3M_5 transitions are energetically forbidden. Experimental results (Sec. II) are listed for comparison.

	Theory			
	(a)	(b)	(c)	Experiment
$_{29}$Cu	7.85	4.10	2.17	~7
$_{30}$Zn	6.06	3.46	2.20	~2.5

$Z=29$. The Coster–Kronig widths $\Gamma(L_2L_3)$ from the Green potential are five times larger than those from the hydrogenic calculation.

A difficulty arises in all Auger transition-probability calculations from the uncertainty in exact electron binding energies in the presence of an inner-shell vacancy. Near the threshold, the radiationless transition rate depends steeply on the continuum-electron energy. The problem is especially severe in the present case, because the energy of L_2-L_3M_{45} Coster–Kronig electrons for atomic numbers 29 and 30 is only $\lesssim 10$ eV. How rapidly the corresponding transition probabilities vary with ejected-electron energy is illustrated in Fig. 4.

The energies E of the Auger and Coster–Kronig electrons were computed according to the relation

$$E = E_{n''l''} - E_{nl} - E_{n'l'} . \quad (1)$$

Here, $E_{n''l''}$ and E_{nl} are neutral-atom binding energies for an electron with the quantum numbers of the initial vacancy and the electron that fills this vacancy in the direct transition, respectively.[45] The binding energy $E_{n'l'}$ of the electron that is ejected in the direct transition is taken to be that of the corresponding electron in a neutral atom of the next-higher atomic number.[43,47,48] (In the exchange transition, the roles of the electrons with quantum numbers nl and $n'l'$ are interchanged.) The binding energies were taken from the ESCA tables of neutral-atom ionization thresholds.[31] The available experimental and theoretical information does not give a clear-cut indication whether L_2-L_3M_{45} Coster–Kronig transitions are allowed or forbidden for $Z=29$ and 30. Consequently, we have computed L_2 Coster–Kronig widths for these two atomic numbers under three different assumptions regarding the energetics (Table II). In case (a), L_2-L_2M_4 and L_2-L_3M_5 transitions are taken to be energetically allowed, and the Coster–Kronig electrons are assumed to have an energy of 10 eV for Cu and 5 eV for Zn. In case (b), only ejection of M_5 electrons is assumed to be possible, with the same kinetic energies as indicated under (a). In case (c), both classes of Coster–Kronig transitions are taken to be energetically impossible.

B. Comparison with Experiment

For comparison with measurements described in Sec. II, we compute the Auger-electron intensity ratio

$$\frac{I(L_3\text{-}M_{45}M_{45})}{I(L_2\text{-}M_{45}M_{45})} = \frac{N_1(f_{13}+f_{12}f_{23})+N_3+N_2f_{23}}{N_1f_{12}+N_2-(N_1f_{12}+N_2)f_{23}} \times \frac{\Gamma(L_3\text{-}M_{45}M_{45})}{\Gamma(L_2\text{-}M_{45}M_{45})} \quad (2)$$

under the assumptions (a), (b), and (c) defined in the preceding paragraph (Table III). These ratios were calculated for an initial L-vacancy distribution $N_1:N_2:N_3=0:1:2$, corresponding to the experimental situation (Sec. II).

The data appear to indicate that assumption (a) correctly describes the energetics for $Z=29$, and assumption (b), for $Z=30$. For copper, we then find a theoretical L_3-$M_{45}M_{45}/L_2$-$M_{45}M_{45}$ Auger-electron intensity ratio of 7.85, in agreement with the measured ratio of ~7; however, the calculated total L_2-level width exceeds the measured width (Table I) by 50%. For zinc, the calculated L_3-$M_{45}M_{45}/L_2$-$M_{45}M_{45}$ Auger-electron intensity ratio of 3.46 exceeds the measured ratio of ~2.5, while the calculated and measured total L_2 widths agree very closely. The discrepancies are traceable to the energetics.

The calculated L_3-level widths (Table II) agree perfectly with the experimental values (Table I), within the errors of measurement.

ACKNOWLEDGMENTS

Two of the authors (L. Y. and I. A.) are indebted to C. Kuyatt and B. Henke for consultations regarding the improvement of the electron spectrometer, E. Fisher and S. Seltzer for computer programs, and T. Tsang for helpful discussions.

*Research supported in part by the U. S. Army Research Office-Durham and the National Aeronautics and Space Administration.

[1]J. H. Scofield, Phys. Rev. **179**, 9 (1969).

[2]J. H. Scofield, Lawrence Livermore Laboratory Report No. UCRL-51231, 1972 (unpublished).

[3]H. R. Rosner and C. P. Bhalla, Z. Phys. **231**, 347 (1970).

[4]E. J. McGuire, Phys. Rev. A **3**, 587 (1971).

[5]M. H. Chen, B. Crasemann, and V. O. Kostroun, Phys. Rev. A **4**, 1 (1971).

[6]B. Crasemann, M. H. Chen, and V. O. Kostroun, Phys. Rev. A **4**, 2161 (1971).

[7]M. H. Chen, B. Crasemann, P. Venugopala Rao, J. M. Palms, and R. E. Wood, Phys. Rev. A **4**, 846 (1971).

[8]D. L. Walters and C. P. Bhalla, Phys. Rev. A **4**, 2164 (1971).
[9]W. Bambynek, B. Crasemann, R. W. Fink, H.-U. Freund, H. Mark, C. D. Swift, R. E. Price, and P. Venugopala Rao, Rev. Mod. Phys. **44**, 716 (1972).
[10]B. Crasemann, in Inner-Shell Ionization Phenomena and Future Applications, edited by R. W. Fink, S. T. Manson, J. M. Palms, and P. Venugopala Rao, U. S. Atomic Energy Commission Report No. CONF- 720404, 1973, p. 9 (unpublished).
[11]J. C. McGeorge, H.-U. Freund, and R. W. Fink, Nucl. Phys. A **154**, 526 (1970).
[12]S. Mohan, H.-U. Freund, R. W. Fink, and P. Venugopala Rao, Phys. Rev. C **1**, 254 (1970).
[13]S. Mohan, R. W. Fink, R. E. Wood, J. M. Palms, and P. Venugopala Rao, Z. Phys. **239**, 423 (1970).
[14]J. M. Palms, R. E. Wood, P. Venugopala Rao, and V. O. Kostroun, Phys. Rev. C **2**, 592 (1970).
[15]R. E. Wood, J. M. Palms, and P. Venugopala Rao, Phys. Rev. **187**, 1497 (1969).
[16]P. Venugopala Rao, R. E. Wood, J. M. Palms, and R. W. Fink, Phys. Rev. **178**, 1997 (1969).
[17]R. E. Wood, J. M. Palms, and P. Venugopala Rao, Phys. Rev. A **5**, 11 (1972).
[18]P. Venugopala Rao, J. M. Palms, and R. E. Wood, Phys. Rev. A **3**, 1568 (1971).
[19]P. Venugopala Rao and B. Crasemann, Phys. Rev. **139**, A1926 (1965).
[20]J. C. McGeorge, S. Mohan, and R. W. Fink, Phys. Rev. A **4**, 1317 (1971).
[21]J. C. McGeorge and R. W. Fink, Z. Phys. **248**, 208 (1971).
[22]J. Byrne, W. Gelletly, M. A. S. Ross, and F. Shaikh, Phys. Rev. **170**, 80 (1968).
[23]J. Byrne, R. J. D. Beattle, S. Benda, and I. Collingwood, J. Phys. B **3**, 1166 (1970).
[24]L. I Yin, T. Tsang, and I. Adler, in Ref. 10, p. 694.
[25]M. O. Krause, F. Wuilleumier, and C. W. Nestor, Jr., Phys. Rev. A **6**, 871 (1972).
[26]L. I Yin, S. Ghose, and I. Adler, J. Geophys. Res. 77, 1360 (1972).
[27]L. I Yin, E. Yellin, and I. Adler, J. Appl. Phys. **42**, 3595 (1971).
[28]K. Siegbahn, D. Hammond, H. Fellner-Feldegg, and E. F. Barnett, Science **176**, 245 (1972).
[29]K. Siegbahn, C. Nordling, G. Johansson, J. Hedman, P. F. Hedén, K. Hamrin, U. Gelius, T. Bergmark, L. O. Werme, R. Manne, and Y. Baer, *ESCA Applied to Free Molecules* (North-Holland, Amsterdam, 1969), pp. 1,17.
[30]L. G. Parratt, Rev. Mod. Phys. **31**, 616 (1959).
[31]K. Siegbahn, C. Nordling, A. Fahlman, R. Nordberg, K. Hamrin, J. Hedman, G. Johansson, T. Bergmark, S. Karlsson, I. Lindgren, and B. Lindberg, *ESCA, Atomic, Molecular and Solid State Structure Studied by Means of Electron Spectroscopy* (Almqvist and Wiksells, Uppsala, 1967).
[32]Y. Baer, P. F. Hedén, J. Hedman, M. Klasson, C. Nordling, and K. Siegbahn, Phys. Scr. **1**, 55 (1970).
[33]L. I Yin, T. Tsang, I. Adler, and E. Yellin, J. Appl. Phys. 43, 3464 (1972).
[34]T. W. Haas, J. T. Grant, and G. J. Dooley, Phys. Rev. B **1**, 1449 (1970).
[35]S. Aksela, M. Pessa, and M. Karras, Z. Phys. **237**, 381 (1970).
[36]J. P. Coad and J. C. Rivière, Z. Phys. **244**, 19 (1971).
[37]J. P. Coad and J. C. Rivière, Surf. Sci. **25**, 609 (1971).
[38]L. H. Jenkins and M. F. Chung, Surf. Sci. **24**, 125 (1971).
[39]R. W. Fink, R. C. Jopson, H. Mark, and C. D. Swift, Rev. Mod. Phys. **38**, 513 (1966).
[40]C. S. Fadley and D. A. Shirley, Phys. Rev. A **2**, 1109 (1970).
[41]G. Wentzel, Z. Phys. **43**, 524 (1927).
[42]A. E. S. Green, D. L. Sellin, and A. S. Zachor, Phys. Rev. **184**, 1 (1969).
[43]V. O. Kostroun, M. H. Chen, and B. Crasemann, Phys. Rev. A **3**, 533 (1971).
[44]M. H. Chen, Ph. D. thesis (University of Oregon, 1972) (unpublished).
[45]M. H. Chen and B. Crasemann, in Ref. 10, p. 43.
[46]F. Herman and S. Skillman, *Atomic Structure Calculations* (Prentice-Hall, Englewood Cliffs, N. J., 1963).
[47]E. J. Callan, Phys. Rev. **124**, 793 (1961).
[48]E. J. Callan, in *Role of Atomic Electrons in Nuclear Transformations* (Nuclear Energy Information Center, Warsaw, 1963), Vol. 3, p. 419.

PHYSICAL REVIEW A VOLUME 7, NUMBER 3 MARCH 1973

Lower Bound to Limiting Fields in Nonlinear Electrodynamics*

Gerhard Soff, Johann Rafelski, and Walter Greiner
Institut für Theoretische Physik der Universität Frankfurt, Frankfurt am Main, Germany
(Received 31 August 1972)

In view of new high-precision experiments in atomic physics it seems necessary to reexamine nonlinear theories of electrodynamics. The precise calculation of electronic and muonic atomic energies has been used to determine the possible size of the upper limit E_{max} to the electric field strength, which has been assumed to be a parameter. This is opposed to Born's idea of a purely electromagnetic origin of the electron's mass which determines E_{max}. We find $E_{max} \geq 1.7 \times 10^{20}$ V/cm.

In recent years nonlinear electrodynamics has not belonged to the mainstream of research because any effective work within this framework was handicapped by mathematical and numerical difficulties with nonlinear equations. As the nonlinear effects were expected to show up in experiments only when high electric fields of the order of 10^{18} V/cm are involved, it was argued that the only possible experiments would be dominated by quantum effects, so that nonlinear effects would be invisible.[1] However, very recent γ-spectroscopic experiments and calculations in atomic